

Uniformity First: Uniformity-aware Test-time Adaptation of Vision-language Models against Image Corruption

Kazuki Adachi^{*‡}, Shin'ya Yamaguchi^{*†}, and Tomoki Hamagami[‡]
^{*}NTT, Inc. [†]Kyoto University [‡]Yokohama National University

Abstract—Pre-trained vision-language models such as contrastive language-image pre-training (CLIP) have demonstrated a remarkable generalizability, which has enabled a wide range of applications represented by zero-shot classification. However, vision-language models still suffer when they face datasets with large gaps from training ones, i.e., distribution shifts. We found that CLIP is especially vulnerable to sensor degradation, a type of realistic distribution shift caused by sensor conditions such as weather, light, or noise. Collecting a new dataset from a test distribution for fine-tuning highly costs since sensor degradation occurs unexpectedly and has a range of variety. Thus, we investigate *test-time adaptation (TTA)* of zero-shot classification, which enables on-the-fly adaptation to the test distribution with unlabeled test data. Existing TTA methods for CLIP mainly focus on modifying image and text embeddings or predictions to address distribution shifts. Although these methods can adapt to domain shifts, such as fine-grained labels spaces or different renditions in input images, they fail to adapt to distribution shifts caused by sensor degradation. We found that this is because image embeddings are “corrupted” in terms of *uniformity*, a measure related to the amount of information. To make models robust to sensor degradation, we propose a novel method called *uniformity-aware information-balanced TTA (UnInfo)*. To address the corruption of image embeddings, we introduce uniformity-aware confidence maximization, information-aware loss balancing, and knowledge distillation from the exponential moving average (EMA) teacher. The uniformity-aware confidence maximization induces image embeddings to uniformly distribute on the unit hypersphere to retain input information along with confidence maximization of predictions. The loss balancing adaptively assigns weights to the losses of uniformity and confidence on the basis of the current classification performance. The knowledge distillation from the EMA teacher stabilizes adaptation and avoids catastrophic forgetting. Through experiments, we demonstrate that our UnInfo improves accuracy under sensor degradation by retaining information in terms of uniformity.

Index Terms—Vision-language models, CLIP, test-time adaptation, sensor degradation, distribution shift.

I. INTRODUCTION

VISION-language models (VLMs) pre-trained on large-scale datasets such as contrastive language-image pre-training (CLIP) [1] and ALIGN [2] have demonstrated remarkable generalizability and rich feature representations. Specifically, pre-trained VLMs have enabled various applications such as zero-shot transfer [1], [3], [4], image/video

retrieval [5], [6], and image generation [7], [8]. VLMs owe their success to their rich feature representations that unify vision and language modalities and public availability of the pre-trained weights such as OpenCLIP [9]–[11] and OpenAI CLIP¹. However, despite their generalizability, VLMs still face a challenge in adapting to distribution shifts, i.e., making predictions on test datasets with large gaps from the training dataset [12]–[21].

A naive way of adapting VLMs is to collect a dataset from the test distribution and fine-tune the model or adjust the head classifier. However, labeled data from the test distribution may not be available because the distribution shift is unknown before deployment [22], [23].

To adapt to distribution shifts instantly after being deployed in the test distribution, *test-time adaptation (TTA)* [24], a paradigm aiming to adapt models during testing using only unlabeled test data, has attracted attention. In the context of VLMs, recent works [15]–[21] have intensively studied the TTA for zero-shot classification, which is one of the most common applications of VLMs. When the domain changes, text prompts can be suboptimal. For example, in an art or illustration domain, text prompt such as “a photo of a [class name]” is not appropriate [15], [25], [26]. In other words, there is a gap between text prompts and images in the embedding space, which is crucial for VLMs’ generalization [27]–[30]. Existing TTA methods for VLMs mainly aim at adapting to domain shifts (also called natural distribution shifts), such as changes in rendition, out-of-distribution (OOD) [31]–[34], or fine-grained zero-shot classification [35], [36] by modifying image and/or text embeddings during testing, which can be viewed as addressing the modality gap.

While existing TTA methods successfully adapt to the domain shifts, they overlook another type of realistic distribution shift: *sensor degradation* [37], [38]. When an image recognition system is deployed in the real world, the model faces various perturbations even in the same domain. This is because of changes in weather, light conditions, noise, cameras, etc., which are crucial in a wide range of applications, such as autonomous driving or surveillance cameras [23], [39]–[42]. Such perturbations occur unexpectedly within a single domain. In the existing literature on ordinary classification models, sensor degradation deteriorates the model’s accuracy [37],

Corresponding author: Kazuki Adachi (kazuki.adachi@ntt.com)

Code is available at <https://github.com/kzkadc/uninfo>.

This work has been submitted to the IEEE for possible publication. Copyright may be transferred without notice, after which this version may no longer be accessible.

¹<https://github.com/openai/CLIP>

[43]. However, the TTA of VLMs against such distribution shifts has not been explored or evaluated in existing works.

To examine whether VLMs are also vulnerable to sensor degradation, we evaluated existing TTA methods for VLMs on image corruption [37], [44] in terms of zero-shot classification performance using CLIP. Through the experiment, we found that CLIP significantly degrades the performance on corrupted images and that existing TTA methods can fail to improve performance. Moreover, we analyzed image embeddings and CLIP’s knowledge about sensor degradation for revealing the difference between domain shift and sensor degradation. As a result, we experimentally found that sensor degradation also causes the modality gap, but the mechanism differs from domain shifts; the modality gap occurs by image embeddings being “corrupted” in terms of *uniformity*, a measure related to the amount of input information retained in the embedding space [45]. In other words, the amount of input information retained in the image embeddings becomes small. This is the key cause of the failure of existing CLIP TTA methods to retain performance. Under sensor degradation, it is challenging to utilize the information that remains in the image embeddings by only modifying them. Further, we found that CLIP models cannot sufficiently encode words related to sensor degradation; thus, simple prompting techniques, such as ensemble or incorporating corruption name to prompts, cannot recover the performance degradation (Section III). From these observations, existing TTA methods or simple prompting techniques suffer from sensor degradation, highlighting the necessity of a novel TTA method suitable for sensor degradation.

To enable the TTA of CLIP under sensor degradation, we propose a novel method called *uniformity-aware information-balanced test-time adaptation (UnInfo)*. UnInfo addresses the fundamental challenge of corrupted image embeddings by updating the image encoder with a low-rank adapter (LoRA) [46]. To realize effective adaptation, UnInfo consists of three components: (i) uniformity-aware confidence maximization, (ii) information-aware loss balancing, and (iii) knowledge distillation from the exponential moving average (EMA) teacher. Uniformity-aware confidence maximization seeks to maximize prediction confidence, as is usually done in existing TTA of general classification models [22], [42], [47]–[50], while incorporating uniformity to prevent embeddings from losing input information. The information-aware loss balancing adaptively controls the balance between confidence maximization and uniformity enhancement on the basis of mutual information so that uniformity is first leveraged and then confidence is addressed. This balancing plays a critical role, specifically when confidence is unreliable because of severe image embedding corruption. The knowledge distillation from the EMA teacher stabilizes the encoder update by tracking the EMA of LoRA parameters and regularizing the student’s prediction to be close to the teacher’s.

Through extensive experiments, our UnInfo improved the test zero-shot accuracy on various sensor degradations by incorporating uniformity and balancing priority between uniformity and entropy.

II. ZERO-SHOT CLASSIFICATION WITH CLIP

Given a pre-trained CLIP composed of a text encoder $f_{\theta_{\text{txt}}}^{\text{txt}} : \mathcal{T} \rightarrow \mathbb{R}^d$ and image encoder $f_{\theta_{\text{img}}}^{\text{img}} : \mathcal{X} \rightarrow \mathbb{R}^d$, we first encode the text prompts to obtain text embeddings, which are used for the prototype of each class in the embedding space \mathbb{R}^d , where \mathcal{T} and \mathcal{X} are text and image input spaces, and θ_{txt} and θ_{img} are pre-trained weights of the encoders. The text prompts typically consist of a template and class names, like “a photo of a [class name],” denoted by \mathbf{p}_c for class c . We denote the corresponding text embeddings as $\{\mathbf{t}_c = f_{\theta_{\text{txt}}}^{\text{txt}}(\mathbf{p}_c)\}_{c=1}^C$, where C is the total number of classes. We assume the text embeddings are normalized, i.e., $\|\mathbf{t}_c\|_2 = 1$.

For a test image $\mathbf{x} \in \mathcal{X}$, we compute the image embedding $\mathbf{z} = f_{\theta_{\text{img}}}^{\text{img}}(\mathbf{x})$, where $\|\mathbf{z}\|_2 = 1$. The similarity between the image and text embeddings $\mathbf{z}^\top \mathbf{t}_c$ is regarded as the logit for class c . The zero-shot prediction probability is obtained by

$$\hat{p}_c = \text{softmax}(\mathbf{z}^\top [\mathbf{t}_1, \dots, \mathbf{t}_C] / \tau)_c, \quad (1)$$

where $\tau > 0$ is the temperature parameter. The final prediction is made by taking the argmax of \hat{p}_c .

III. PRELIMINARY EXPERIMENT

First, we empirically demonstrate the vulnerability of CLIP under sensor degradation in terms of zero-shot classification accuracy. Moreover, CLIPs cannot properly encode images under such distribution shifts, i.e., the performance degradation cannot be recovered by simple prompting techniques because CLIPs cannot sufficiently represent concepts related to image quality.

We evaluated a ViT-B/16 CLIP pre-trained on the LAION dataset [11] downloaded via OpenCLIP [9]. We used the ImageNet-C [37] dataset, which includes 15 types of image corruption simulating the sensor degradation (see Section V-A for dataset details). We performed zero-shot classification with the text prompt “a photo of a [class name]” (Normal prompt). We also used the ensemble of 80 text prompts, e.g., “a bad photo of a [class name],” “a photo of many [class name],” and so on, which is widely adopted as one baseline [1] (Ensemble), to see the effectiveness of prompt engineering on sensor degradation. To check the expressiveness of CLIP representation, we also examined text prompts that included descriptions of corruption. Specifically, we used the prompts “a photo of a [class name] corrupted by [corruption name].” For each corruption, we generated ten synonyms of the corruption name with GPT-4o [51] and ensembled the text prompts (Corruption prompt). Details of the prompt ensemble are provided in the appendix. We tested on ImageNet [52], ImageNet-A/R [31], [33] (domain shifts), and ImageNet-C [37] to observe the effect of sensor degradation.

Table I shows the accuracy, entropy, uniformity loss, and the modality gap between text and image embeddings by the earth mover’s distance (EMD) on the datasets. The entropy measures the uncertainty of predictions (a lower value indicates high confidence), and the uniformity loss measures how image embeddings are uniformly distributed on the unit hypersphere, which is related to the amount of input information preserved

TABLE I
ZERO-SHOT CLASSIFICATION METRICS OF ViT-B/16 CLIP WITH SIMPLE PROMPTING TECHNIQUES ON IMAGENET FAMILY AND IMAGENET-C. ‘‘CLEAN’’
CORRESPONDS TO THE IMAGENET.

Metric	ImageNet	ImageNet-A	ImageNet-R	Domain shift Mean	Defocus	Glass	Motion	Zoom	Contrast	Elastic	Jpeg	Pixelate	Gaussian	Impulse	Shot	Brightness	Fog	Frost	Snow	Corruption
					blur	blur	blur	blur		transform	compression		noise	noise		noise				
Accuracy (Normal prompt, \uparrow)	66.97	32.91	74.36	58.08	28.18	11.81	19.13	17.65	17.90	13.37	36.77	36.92	6.02	6.12	7.88	54.75	34.39	27.32	27.77	23.06
Accuracy (Ensemble, \uparrow)	67.59	33.15	76.51	59.08	29.09	12.56	20.56	19.12	18.55	14.34	37.71	37.89	6.36	6.54	8.27	55.78	35.99	28.37	28.34	23.97
Accuracy (Corruption prompt, \uparrow)	-	-	-	-	26.53	12.15	18.39	17.99	17.65	13.96	36.29	36.35	6.02	6.10	7.80	53.93	33.43	27.34	26.55	22.70
Entropy (\downarrow)	0.748	1.220	0.595	0.854	2.011	2.703	2.317	2.245	3.247	2.297	1.632	1.615	3.773	3.714	3.671	1.061	1.681	1.905	2.048	2.395
Uniformity loss (\downarrow)	0.513	0.538	0.500	0.517	0.682	0.735	0.722	0.715	0.744	0.706	0.630	0.641	0.855	0.853	0.839	0.601	0.665	0.655	0.686	0.715
Modality gap (EMD, \downarrow)	1.291	1.333	1.348	1.324	1.298	1.326	1.325	1.327	1.337	1.341	1.293	1.296	1.299	1.297	1.296	1.293	1.307	1.315	1.308	1.311

TABLE II
ZERO-SHOT CORRUPTION TYPE CLASSIFICATION ACCURACY (%).

Defocus blur	Glass blur	Motion blur	Zoom blur	Contrast	Elastic transform	Jpeg compression	Pixelate	Gaussian noise	Impulse noise	Shot noise	Brightness	Fog	Frost	Snow	Total
68.76	11.12	75.61	2.61	0.36	18.91	1.28	8.64	30.28	0.23	0.70	3.43	78.95	49.16	7.32	23.53

in the image embedding [53] (a lower value indicates more information is preserved). The entropy and uniformity loss are defined as follows:

$$\text{Entropy} = \sum_{c=1}^C -\hat{p}_c \log \hat{p}_c, \quad (2)$$

$$\text{Uniformity loss} = \mathbb{E}_{\mathbf{z}_1, \mathbf{z}_2} [\exp(-\|\mathbf{z}_1 - \mathbf{z}_2\|_2^2)]. \quad (3)$$

On the domain shifts, the normal prompt and ensemble had 1%pt accuracy improvement on average. On the other hand, ImageNet-C significantly degrades accuracy, and the ensemble did not result in significant improvement. Moreover, including corruption information in the prompt (Corruption prompt) resulted in accuracy degradation. The remarkable difference is that the entropy and uniformity loss significantly increased compared to the domain shifts on all corruption types, while there is no significant difference in the modality gap. In other words, the prediction becomes uncertain, and information preserved in the image embeddings decreases. Thus, sensor degradation, such as image corruption, can distort the semantical alignment between image and text embeddings, but the cause of the gap differs from the domain shift. This is because ViTs or CNNs, which are typically used for image encoders, are vulnerable to such distribution shifts [37], [43]. This phenomenon can be explained as follows: the sensor degradation can be considered as a Markov chain $X \rightarrow X' \rightarrow Z$, where X , X' , and Z are the original clean image, its corrupted one, and the image embedding of X' , respectively. According to the data processing inequality, $\mathcal{I}(X; Z) \leq \mathcal{I}(X; X')$, where $\mathcal{I}(\cdot; \cdot)$ is the mutual information. By rewriting the mutual information, we have

$$\mathcal{H}(Z) - \mathcal{H}(Z|X) \leq \mathcal{H}(X) - \mathcal{H}(X|X'), \quad (4)$$

where $\mathcal{H}(\cdot)$ is the entropy. When an image is severely corrupted, the original image X is difficult to predict from the corrupted one X' , i.e., $\mathcal{H}(X|X')$ increases, resulting in the

right-hand side being smaller. In the left-hand side, $\mathcal{H}(Z|X)$ can be regarded as a constant since the CLIP’s image encoder is deterministic. Thus, the upper bound of $\mathcal{H}(Z)$ becomes smaller, i.e., Z will have less uniformity. Hence, uniformity is a key factor in sensor degradation.

Next, to check whether the CLIP recognizes image corruption types, we performed zero-shot classification of the 15 corruption types of input images instead of object categories using the text prompts ‘‘a photo corrupted by [corruption name].’’ Table II shows the results. Most corruption types had poor accuracies, which suggests that CLIP cannot recognize image corruption types. Even in the cases of corruption types with high accuracies (such as defocus blur, motion blur, and fog), the contribution of including the corruption information for object classification is limited or even worse, as shown in Table I.

From these observations, sensor degradation causes the modality gap as well as domain shifts, but has different properties from domain shifts in terms of the uniformity and entropy, which suggests that the CLIP cannot properly encode images corrupted by the sensor degradation. Moreover, performance improvement by simple prompting techniques is limited under the sensor degradation.

IV. UNIFORMITY-AWARE INFORMATION-BALANCED TEST-TIME ADAPTATION

We introduce our proposed method, *Uniformity-aware Information-balanced Test-time Adaptation (UnInfo)*. Figure 1 illustrates the overview of UnInfo. The goal of TTA is to perform zero-shot classification on each incoming batch of test images $\{\mathbf{x}_i\}_{i=1}^B$ by updating the model parameters to make accurate predictions, where B is the batch size. Since we focus on sensor degradation of input images, we specifically update θ_{img} in our method.

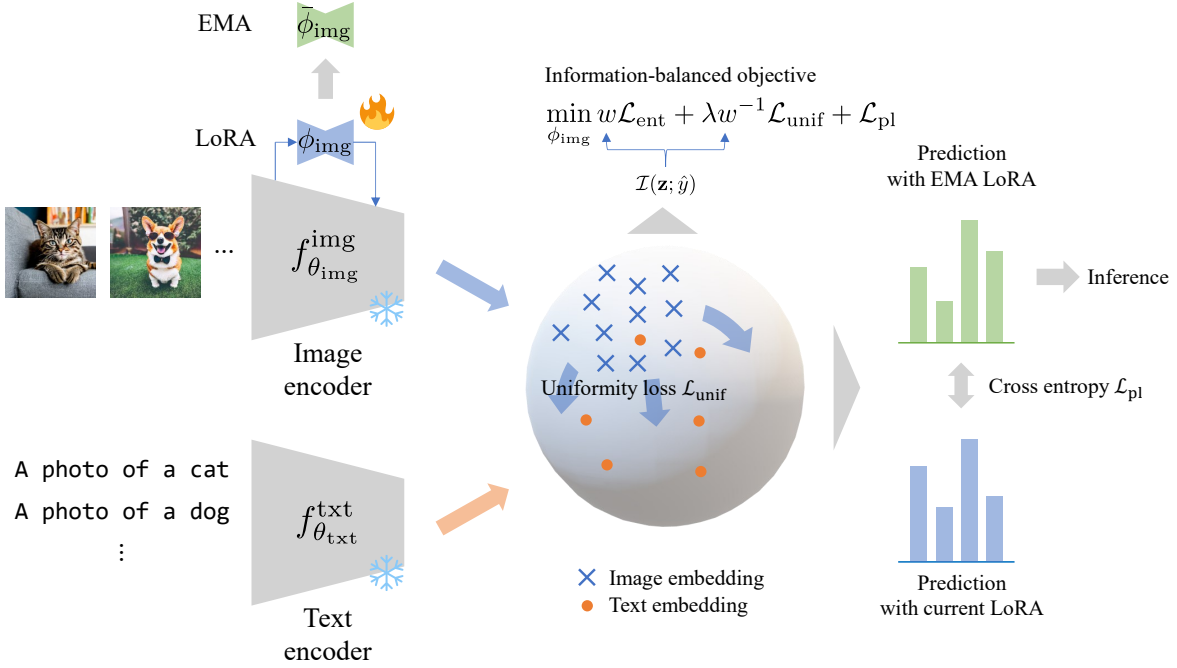


Fig. 1. Overview of Uniformity-aware Information-balanced Test-time Adaptation (UnInfo).

A. Uniformity-aware Confidence Maximization

Our method’s basic approach is to maximize predictions’ confidence in entropy, which is widely adopted in existing TTA methods for general classification models [22], [23], [42], [47]–[50]. In zero-shot classification with CLIP, the entropy loss is computed by using the prediction probability \hat{p}_c on the basis of similarity, defined in Equation (1):

$$\mathcal{L}_{\text{ent}} = \frac{1}{B} \sum_{i=1}^B \sum_{c=1}^C -\hat{p}_{i,c} \log \hat{p}_{i,c}. \quad (5)$$

Entropy is a promising proxy for classification accuracy when the images are appropriately embedded and input information is preserved, e.g., under natural distribution shifts. However, the amount of input information preserved in the image embeddings decreases under sensor degradation as the entropy and uniformity loss increase in Table I, as discussed in Section III.

In such cases, the improvement by solely minimizing the entropy is limited since it attempts to leverage less information. For making input information retained in the embedding space, we minimize the uniformity loss [53] along with the entropy:

$$\mathcal{L} = \mathcal{L}_{\text{ent}} + \lambda \mathcal{L}_{\text{unif}}, \quad (6)$$

$$\mathcal{L}_{\text{unif}} = \log \frac{1}{B^2} \sum_{i=1}^B \sum_{j=1}^B \exp(-\|\mathbf{z}_i - \mathbf{z}_j\|_2^2), \quad (7)$$

where $\lambda > 0$ is a hyperparameter, and $\mathbf{z}_i, \mathbf{z}_j$ are image embeddings of a batch of input images.

B. Information-aware Loss Balancing

As described in Sections III and IV-A, minimizing the uniformity loss helps retain input information of image em-

beddings. However, we found that the importance of uniformity and entropy can dynamically change during TTA. For example, entropy should be prioritized when zero-shot classification works well, e.g., when sensor degradation is not severe. In fact, we observed that uniformity differs depends on corruption types in the preliminary experiment in Table I. On the other hand, uniformity loss should be leveraged first, and then entropy should be addressed when zero-shot classification becomes a degenerated solution, e.g., classifying all images into a single class under severe sensor degradation.

To recognize the current regime and adaptively assign weights to the entropy and uniformity loss, we propose *information-aware loss balancing*. We employ the mutual information between the image embedding \mathbf{z} and prediction \hat{y} , denoted by $\mathcal{I}(\mathbf{z}; \hat{y})$, to detect whether classification works without supervision. We assign the weights to the two losses as follows:

$$\mathcal{L} = w \mathcal{L}_{\text{ent}} + \lambda w^{-1} \mathcal{L}_{\text{unif}}, \quad (8)$$

$$w = \exp(\mathcal{I}(\mathbf{z}; \hat{y}) - \mathcal{I}_0), \quad (9)$$

where \mathcal{I}_0 is a hyperparameter to determine the threshold between the two regimes. The mutual information $\mathcal{I}(\mathbf{z}; \hat{y})$ is widely used in representation learning for measuring the quality of features and is computed as follows [54]–[57]:

$$\begin{aligned} \mathcal{I}(\mathbf{z}; \hat{y}) &= \mathcal{H}(\mathbf{z}) - \mathcal{H}(\mathbf{z}|\hat{y}) \\ &= \sum_{c=1}^C -\bar{p}_c \log \bar{p}_c - \frac{1}{B} \sum_{i=1}^B \sum_{c=1}^C -\hat{p}_{i,c} \log \hat{p}_{i,c}, \end{aligned} \quad (10)$$

where $\mathcal{H}(\cdot)$ is entropy and $\bar{p}_c = (1/B) \sum_{i=1}^B \hat{p}_{i,c}$. Intuitively, $\mathcal{I}(\mathbf{z}; \hat{y})$ takes small values when the image embedding \mathbf{z} is less diverse and predictions are not confident. In such a case, $\mathcal{L}_{\text{unif}}$ is assigned more significant weight to make the image

embeddings diverse and retain more information. On the other hand, \mathcal{L}_{ent} is leveraged to make predictions more confident. Note that gradients are not propagated to the weight w since the balance is not an objective to be optimized.

C. Update with Low-rank Adapters

Although we aim to update the image encoder $f_{\theta_{\text{img}}}^{\text{img}}$ to minimize the proposed loss in Equation (8), updating the whole θ_{img} naively leads to catastrophic model forgetting [58], [59]. To avoid this, we fix the original pre-trained parameter θ_{img} and add the LoRA [46] to the linear weights in the attention layers, inspired by Zanella & Ayed [60]. Specifically, given an attention layer at the l -th layer

$$\mathbf{h}^{l+1} = \text{softmax} \left((W_Q^l \mathbf{h}^l)(W_K^l \mathbf{h}^l)^\top / \sqrt{d^l} \right) W_V^l \mathbf{h}^l, \quad (11)$$

we attach low-rank matrices to W^l :

$$W^l \rightarrow W^l + A^l B^l, \quad (12)$$

where $A^l \in \mathbb{R}^{d^l \times d_{\text{LoRA}}}$ and $B^l \in \mathbb{R}^{d_{\text{LoRA}} \times d^l}$ ($d_{\text{LoRA}} < d^l$). We denote the LoRA parameters as ϕ_{img} .

D. Knowledge Distillation from EMA Teacher

For stabilizing the adaptation, we track the EMA of ϕ_{img} following previous works [61]–[64]. That is, we update $\bar{\phi}_{\text{img}}$ in every iteration:

$$\bar{\phi}_{\text{img}} \leftarrow m \phi_{\text{img}} + (1 - m) \bar{\phi}_{\text{img}}, \quad (13)$$

where $m \in (0, 1)$ is the momentum parameter. We adopt predictions made with $\bar{\phi}_{\text{img}}$ for inference. Using $\bar{\phi}_{\text{img}}$ as the teacher, we penalize the current LoRA parameters ϕ_{img} (student) to make predictions close to those of the teacher. Specifically, we take the cross entropy between the teacher and student outputs [61], [62]:

$$\mathcal{L}_{\text{pl}} = \frac{1}{B} \sum_{i=1}^B \sum_{c=1}^C -\hat{q}_{i,c} \log \hat{p}_{i,c}, \quad (14)$$

where $\hat{p}_{i,c}$ is the student’s output defined in Equation (1), and $\hat{q}_{i,c}$ is the teacher’s output computed in the same way with $\hat{p}_{i,c}$ but using the EMA parameter $\bar{\phi}_{\text{img}}$.

To sum up Sections IV-A to IV-D, our objective is as follows:

$$\min_{\phi_{\text{img}}} w \mathcal{L}_{\text{ent}} + \lambda w^{-1} \mathcal{L}_{\text{unif}} + \mathcal{L}_{\text{pl}}, \quad (15)$$

where each element is defined in Equations (5), (7), (9) and (14). Algorithm 1 lists the procedure of UnInfo.

V. EXPERIMENT

We conducted experiments on TTA under datasets that include sensor degradation.

Algorithm 1 Procedure of UnInfo.

Input: Pre-trained image encoder $f_{\theta_{\text{img}}}^{\text{img}}$, class text embeddings $\{\mathbf{t}_c\}_{c=1}^C$, initialized LoRA ϕ_{img} , target dataset \mathcal{D}

Output: Adapted LoRA parameter (EMA) $\bar{\phi}_{\text{img}}$

for mini-batch $\{\mathbf{x}_i\}_{i=1}^B$ in \mathcal{D} **do**

 Compute image embeddings with the current LoRA
 $\{\mathbf{z}_i = f_{\theta_{\text{img}}, \phi_{\text{img}}}^{\text{img}}(\mathbf{x}_i)\}_{i=1}^B$.

 Compute zero-shot prediction probabilities $\{\hat{p}_{i,c}\}_{i=1}^B$ in accordance with Equation (1).

 Compute teacher zero-shot prediction probabilities $\{\hat{q}_{i,c}\}_{i=1}^B$ using the EMA LoRA $\bar{\phi}_{\text{img}}$.

 Compute the loss in accordance with Equation (15).

 Update ϕ_{img} .

 Update EMA teacher $\bar{\phi}_{\text{img}}$ in accordance with Equation (13).

end for

A. Datasets

ImageNet-C [37]: This dataset is constructed to evaluate the robustness of vision models. It consists of the corrupted version of the validation set of ImageNet [52]. ImageNet-C includes 15 types of corruption, such as blur or digital noise. Each corruption type has five severity levels. We used the images corrupted at the highest severity level.

ImageNet-C-bar [44]: This dataset is constructed to evaluate the robustness of the vision models on a broader range of corruption types. Like ImageNet-C, it also consists of the corrupted version of the ImageNet validation set. ImageNet-C-bar includes 10 corruption types that are algorithmically selected to be dissimilar from ImageNet-C. We used the images corrupted at the highest severity level, as in the ImageNet-C case.

B. Implementation

We used the ViT-B/16 CLIP pre-trained on the DataComp-1B dataset [65]. We downloaded the pre-trained weights via OpenCLIP [10]². We set the temperature of the zero-shot prediction $\tau = 0.01$. For our UnInfo, we used the AdamW optimizer [66] with learning rate = 0.001, weight decay = 0.01, and batch size = 64. We set the weight of the uniformity loss $\lambda = 1$ and the threshold of the information-aware loss balancing weight $\mathcal{I}_0 = 3$. We chose these hyperparameters by using a few corruption types in ImageNet-C and used the selected hyperparameters for the others as default. For the LoRA in UnInfo, we used the implementation provided by Zanella & Ayed [60]³. We set the LoRA hyperparameters, such as α and the rank d_{LoRA} , to the default values and the momentum m of EMA to 0.001. The LoRA matrices A^l and B^l are initialized by the Kaiming uniform initialization [67] and zero, respectively, so that the image encoder outputs are unaffected by random ϕ_{img} at the initial state.

²https://github.com/mlfoundations/open_clip

³<https://github.com/MaxZanella/CLIP-LoRA>

TABLE III

TEST ACCURACY (%) ON IMAGENET-C. THE NUMBERS (1), (5), AND (10) PRESENTED WITH THE METHOD NAMES ARE THE SHOT NUMBERS PER CLASS n USED FOR THE FEW-SHOT ADAPTATION METHODS.

Method	Defocus blur	Glass blur	Motion blur	Zoom blur	Contrast	Elastic transform	Jpeg compression	Pixelate	Gaussian noise	Impulse noise	Shot noise	Brightness	Fog	Frost	Snow	Mean
No-adapt	28.31	11.89	19.16	17.61	17.87	13.22	36.79	37.01	6.08	6.17	7.85	54.89	34.55	27.35	27.67	23.09
Linear probing (1)	11.53	6.15	8.79	9.02	5.87	8.17	15.57	16.36	2.79	2.76	3.41	27.05	16.43	9.88	11.87	10.38
Linear probing (5)	19.55	10.53	15.16	15.25	10.04	14.47	25.68	27.02	4.76	4.95	5.62	43.28	26.10	17.31	19.48	17.28
Linear probing (10)	23.84	12.72	17.97	18.57	12.45	17.69	30.50	32.32	5.78	6.04	6.83	49.90	31.15	21.49	23.63	20.73
Tip-adapter [12] (1)	19.00	9.09	13.92	14.04	9.53	12.60	26.98	27.19	4.06	4.02	5.15	44.92	25.99	18.10	19.28	16.92
Tip-adapter (5)	23.43	12.27	17.61	17.76	11.56	16.82	30.87	32.09	4.88	4.86	6.03	49.88	30.59	21.43	22.82	20.19
Tip-adapter (10)	26.11	13.99	19.85	20.23	12.99	19.26	33.03	34.60	5.52	5.82	6.82	52.40	33.15	24.01	24.83	22.17
TPT [15]	29.66	12.87	21.11	20.54	20.11	15.21	39.27	41.14	6.48	6.74	8.50	57.35	37.05	29.81	30.23	25.07
ZERO [68]	26.85	8.86	18.11	19.89	16.46	12.38	35.09	37.44	3.69	5.33	4.43	53.35	33.50	26.56	27.42	21.96
MTA [19]	27.79	11.29	19.25	18.88	21.18	13.92	37.23	38.95	2.41	2.87	2.96	53.56	34.32	28.02	28.66	22.75
TDA [17]	30.13	14.59	22.10	21.09	19.59	17.15	38.58	39.53	7.23	7.45	9.34	56.99	38.09	30.24	31.02	25.54
UnInfo (ours)	31.51	16.76	23.47	20.40	22.81	16.59	42.03	42.38	7.56	10.60	11.36	57.75	39.16	31.65	32.40	27.10

C. Baseline

We compared our UnInfo with existing TTA methods for CLIP zero-shot classification and few-shot adaptation methods. For few-shot methods, we split $n \in \{1, 5, 10\}$ test samples per class, used them for adaptation, and then tested the model on test samples that were not used for adaptation.

No-adapt: Just performs zero-shot classification without adaptation.

LP (Linear probing): Trains a linear classifier head with few-shot labeled samples from the test set.

Tip-adapter [12]: Modifies predictions by using cached features and logits of few-shot labeled samples from the test set.

TPT (Test-time prompt tuning) [15]: Updates the text token embeddings corresponding to the words of a text template, e.g., “a photo of a,” to minimize the marginal entropy over augmented views of an input image.

TDA (Training-free dynamic adapter) [17]: Constructs positive and negative caches on the basis of prediction confidence on incoming test images and modifies predictions of subsequent inputs.

ZERO [68]: Performs voting within predictions of augmented views of an input image.

MTA (MeanShift for test-time augmentation) [19]: Selects reliable image embeddings among augmented views and modifies the image embedding.

D. Results

1) *Adaptation Performance:* We evaluated each corruption type’s test classification accuracy on ImageNet-C and ImageNet-C-bar. We ran TTA three times with different random seeds for each method and corruption, and report the mean score. Tables III and IV show the results. We can see that our UnInfo consistently surpasses the zero-shot baselines. Intriguingly, the baselines, even the few-shot methods that use labeled test samples for adaptation, sometimes underperformed No-adapt. This is because the baseline methods aim to refine text and/or image embeddings in a post-hoc manner during testing. While corrupted images are not appropriately encoded,

as discussed in Section III, the encoders themselves remain fixed. In contrast, UnInfo successfully adapts to image corruptions by updating the image encoder with LoRA. Specifically, UnInfo significantly improved the accuracy on difficult corruption types in terms of uniformity listed in Table I, e.g., blur and noise, where the amount of information retained in image embeddings is smaller than for other corruption types.

2) *Ablation Study:* Here, we examined the effect of each component in UnInfo: uniformity-aware confidence maximization, information-aware loss balancing, and knowledge distillation from the EMA teacher. Tables V and VI show the results. Minimizing only the entropy loss \mathcal{L}_{ent} resulted in catastrophically poor accuracy in all cases. This is because image corruption affects uniformity, as observed in Section III; solely minimizing entropy can assign unreasonably high confidence to wrong classes by overfitting quickly. In contrast, incorporating the knowledge distillation loss \mathcal{L}_{pl} drastically improved the stability. The uniformity loss $\mathcal{L}_{\text{unif}}$ further improved accuracy compared to $\mathcal{L}_{\text{ent}} + \mathcal{L}_{\text{pl}}$. However, its improvement is sometimes marginal because it overlooks the balance between entropy and uniformity, as Section IV-B describes. Thus, adding the balancing further improved accuracy by properly enhancing entropy or uniformity. Specifically, we observed significant improvements in difficult corruption types that produce high uniformity loss, such as noise corruption. In such cases, uniformity should be recovered first before minimizing entropy loss. UnInfo successfully controls the priority of the losses.

3) *Sensitivity Analysis:* Figure 2 plots the sensitivity analysis of the hyperparameters of UnInfo. We changed the weight of the uniformity loss λ in Equation (8) and the threshold of the mutual information \mathcal{I}_0 for the loss balancing in Equation (9). We ran UnInfo on the ImageNet-C corruptions and reported the average test accuracy. Increasing λ produces better accuracies, mainly in $0.0 \leq \lambda \leq 0.75$, suggesting the efficacy of the uniformity loss, and further increasing λ beyond 1.0 results in slightly higher accuracy. On the other hand, varying \mathcal{I}_0 hits the best accuracy when $\mathcal{I}_0 = 2.75$

TABLE IV
TEST ACCURACY (%) ON IMAGENET-C-BAR. THE NUMBERS (1), (5), AND (10) PRESENTED WITH THE METHOD NAMES ARE THE SHOT NUMBERS PER CLASS n USED FOR THE FEW-SHOT ADAPTATION METHODS.

Method	Blue noise sample	Brownish noise	Caustic refraction	Checkerboard cutout	Cocentric sine waves	Inverse sparkles	Perlin noise	Plasma noise	Single frequency greyscale	Sparkles	Mean
No-adapt	21.87	46.66	39.55	45.51	10.05	19.57	51.21	20.69	16.10	50.00	32.12
Linear probing (1)	9.05	24.22	17.77	21.99	3.74	8.59	24.87	10.04	4.23	26.19	15.07
Linear probing (5)	15.45	38.05	29.12	35.58	6.89	14.28	39.24	15.43	6.82	40.55	24.14
Linear probing (10)	18.58	44.03	34.96	41.54	8.83	17.36	45.82	18.41	9.05	47.20	28.58
Tip-adapter [12] (1)	14.95	37.35	29.99	35.58	7.12	14.82	40.06	15.46	10.06	41.29	24.67
Tip-adapter (5)	18.41	43.08	34.86	40.79	8.37	17.58	45.58	18.15	10.24	46.44	28.35
Tip-adapter (10)	20.22	45.93	37.59	43.65	9.77	19.62	48.52	20.07	11.51	49.26	30.61
TPT [15]	24.63	49.86	42.53	46.36	10.96	21.93	54.31	23.16	17.43	52.20	34.34
ZERO [68]	25.65	45.60	41.14	45.30	10.59	22.79	49.76	20.42	19.81	45.81	32.69
MTA [19]	23.75	45.13	40.28	45.05	9.93	20.53	50.50	20.04	19.32	45.89	32.04
TDA [17]	24.53	50.30	42.90	49.85	12.69	22.56	53.89	24.75	17.77	55.00	35.42
UnInfo (ours)	26.78	51.21	43.73	50.03	12.49	23.58	55.22	24.88	19.67	53.74	36.13

TABLE V
ABLATION OF UNINFO ON IMAGENET-C.

Method	Defocus blur	Glass blur	Motion blur	Zoom blur	Contrast	Elastic transform	Jpeg compression	Pxellate	Gaussian noise	Impulse noise	Shot noise	Brightness	Fog	Frost	Snow	Mean
\mathcal{L}_{ent}	0.10	0.10	0.10	0.10	0.10	0.10	0.10	0.10	0.10	0.10	0.10	0.10	0.10	0.10	0.10	0.10
$\mathcal{L}_{ent} + \mathcal{L}_{pl}$	30.63	15.56	22.61	19.54	21.83	15.99	41.03	40.82	3.31	6.68	8.06	57.17	37.78	30.84	31.29	25.54
$\mathcal{L}_{ent} + \mathcal{L}_{unif} + \mathcal{L}_{pl}$	31.08	16.48	23.40	20.32	22.49	16.67	41.26	41.26	3.90	7.87	7.17	57.24	38.74	31.24	32.01	26.07
$\mathcal{L}_{ent} + \mathcal{L}_{unif} + \mathcal{L}_{pl} + \text{Balancing (UnInfo)}$	31.51	16.76	23.47	20.40	22.81	16.59	42.03	42.38	7.56	10.60	11.36	57.75	39.16	31.65	32.40	27.10

TABLE VI
ABLATION OF UNINFO ON IMAGENET-C-BAR.

Method	Blue noise sample	Brownish noise	Caustic refraction	Checkerboard cutout	Cocentric sine waves	Inverse sparkles	Perlin noise	Plasma noise	Single frequency greyscale	Sparkles	Mean
\mathcal{L}_{ent}	0.10	0.10	0.10	0.10	0.10	0.10	0.10	0.10	0.10	0.10	0.10
$\mathcal{L}_{ent} + \mathcal{L}_{pl}$	26.20	49.67	42.81	48.87	11.67	22.78	53.94	23.85	19.48	49.63	34.89
$\mathcal{L}_{ent} + \mathcal{L}_{unif} + \mathcal{L}_{pl}$	26.75	50.28	43.14	49.59	12.08	23.36	54.47	24.27	19.69	54.27	35.79
$\mathcal{L}_{ent} + \mathcal{L}_{unif} + \mathcal{L}_{pl} + \text{Balancing (UnInfo)}$	26.78	51.21	43.73	50.03	12.49	23.58	55.22	24.88	19.67	53.74	36.13

but slightly affects the accuracy within $2.0 \leq \mathcal{I}_0 \leq 3.25$. However, increasing \mathcal{I}_0 too much deteriorates the accuracy because it controls the bias of the balance between entropy and uniformity. When \mathcal{I}_0 is too high, the uniformity loss is constantly overweighted, and the entropy is no longer optimized.

4) *Computational Efficiency*: Table VII shows each method’s throughput (images per second) and GPU memory usage (MiB). The baseline methods based on marginal confidence over augmented views of an input (TPT [15], ZERO [68], and MTA [19]) had very low throughput because they needed to run forward passes for 64 augmented views per image. TPT and MTA had the lowest throughput because they require a further backward pass and solve an optimization problem for each image, respectively. Especially, TPT had the highest GPU memory usage because of backward pass

TABLE VII
MEAN ADAPTATION THROUGHPUT AND GPU MEMORY USAGE.

Method	Throughput (images/sec.)	GPU memory (MiB)
No-adapt	299.6 ± 1.0	1348
TPT	1.8 ± 0.0	14409
ZERO	4.2 ± 0.0	2319
MTA	1.3 ± 0.0	2331
TDA	44.6 ± 2.4	1414
UnInfo (ours)	73.7 ± 0.5	11736

for prompt optimization. In contrast, UnInfo had the highest throughput since it does not require data augmentation and only requires one forward and backward pass per image while it had the second-highest GPU memory usage. Moreover, the knowledge of the test distribution is accumulated in the

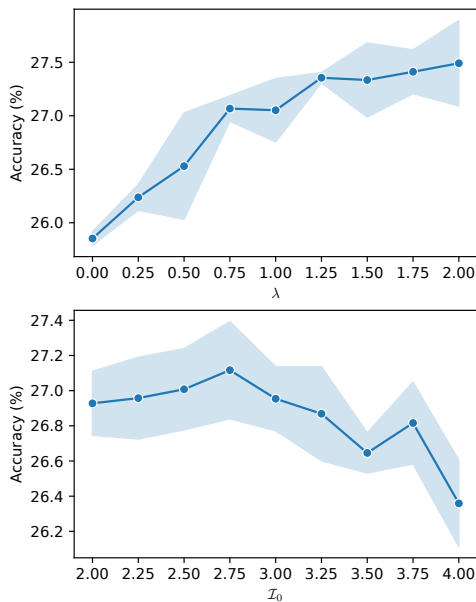


Fig. 2. Sensitivity analysis on the weight of the uniformity loss λ (top) and threshold of the mutual information used in the loss balancing \mathcal{I}_0 (bottom). The mean and standard deviation of the test accuracy calculated over the ImageNet-C corruptions are plotted.

LoRA adapters in UnInfo. Thus, one may stop adaptation and merge LoRA to the stem model when the test distribution is stable. This can further speed up inference and save GPU memory as much as No-adapt. In contrast, TPT, ZERO, and MTA are episodic methods, i.e., they do not update the model or accumulate any information. Thus, they always have to perform adaptation and inference together, unlike UnInfo.

5) *Qualitative Analysis*: Figure 3 plots the evolution of the information-aware loss balancing weights w and w^{-1} in Equation (9). For easy image corruption for which No-adapt produced relatively high accuracy, such as brightness in (a), the weight for the entropy quickly increased, and the weight for uniformity loss was suppressed. This is because image embeddings under the brightness corruption retain information for classification; solely addressing entropy can improve accuracy. The defocus blur in (b) and elastic transform in (c) also showed similar evolutions in which the entropy quickly increases. However, the maximum value of the weight for entropy differs, and the weight for the uniformity loss is retained. This suggests the uniformity loss needs to be minimized along with entropy to retain information for these corruptions. On the other hand, the Gaussian noise in (d) showed a different evolution: the weight is larger for uniformity loss than for the entropy in the initial phase, indicating that retaining information of image embeddings is prioritized.

Next, we visualized embeddings to observe how the uniformity is improved. As the CLIP’s embeddings are normalized and distributed on a unit hypersphere, we used the spherical PCA [69], which projects data points on a high-dimensional unit hypersphere onto a low-dimensional hypersphere (a 2D circle here). Figure 4 visualizes the image embeddings before and after TTA with UnInfo on several corruptions of ImageNet-C, along with the text embeddings. After TTA,

the image embeddings are distributed in a broader range of the circle than those before TTA on all corruptions, which suggests that the uniformity is improved. Moreover, the distributions of image and text embeddings are aligned after TTA, which suggests that the image embeddings become more classification-friendly. Uniformity improved most significantly in the Gaussian noise corruption in (d) because uniformity loss was prioritized by the information-aware loss balancing, as shown in Figure 3 (d), as we intended. On the other hand, uniformity improved less significantly in the brightness corruption in (a) than in the other corruptions since the entropy is highly prioritized for the brightness corruption in Figure 3 (a). In other words, uniformity is less important for this corruption because the image embeddings are already spread in a broader range than for the other corruptions, and their distribution is already aligned with that of the text embeddings before TTA.

VI. RELATED WORK

A. Contrastive Language-image Pre-training

CLIP [1] is a multimodal foundation model training paradigm, especially between image and text modalities. In CLIP, two encoders (an image encoder and a text encoder), are trained to map image and text inputs into a unified embedding space so that semantically corresponding inputs are encoded into close embeddings and vice versa. CLIP is trained on large-scale image-text pair datasets such as LAION [11] and COCO-Caption [70] with InfoNCE loss [53], which promotes encoded features of correct image-text pairs to be similar while incorrect pairs are dissimilar. Although the training strategy is simple, CLIP has demonstrated remarkable generalization on downstream tasks by being trained on a huge dataset (e.g., hundreds of millions of image-text pairs). However, CLIP degrades downstream performance when faced with datasets with a large gap from the training dataset [12]–[21]. Retraining is often infeasible for adapting CLIP to a new dataset because it incurs a substantial computational cost, as described above. To address this challenge, TTA of CLIP has been actively studied.

B. Test-time Adaptation of Vision-language Models

For instantly adapting to test distributions without incurring heavy computational costs, TTA of zero-shot classification with CLIP has been studied. TTA aims to adapt a zero-shot CLIP classifier to the test distribution with only unlabeled test data. The representative approach of CLIP TTA is to update the image and/or text embeddings. Test-time prompt tuning (TPT) [15], [71] updates the text token embeddings (e.g., four embedding vectors corresponding to words of a prompt template “a photo of a”) during testing to minimize the prediction entropy marginalized with augmented views of an input image. The text embedding corresponding to each class is updated to be more appropriate to the current domain by updating the text token embeddings. Existing method also directly update the embeddings or logits computed from the similarity of image and text embeddings TDA [17] and DMN [18] accumulate test inputs and construct the image embedding caches to modify subsequent inputs’ predictions.

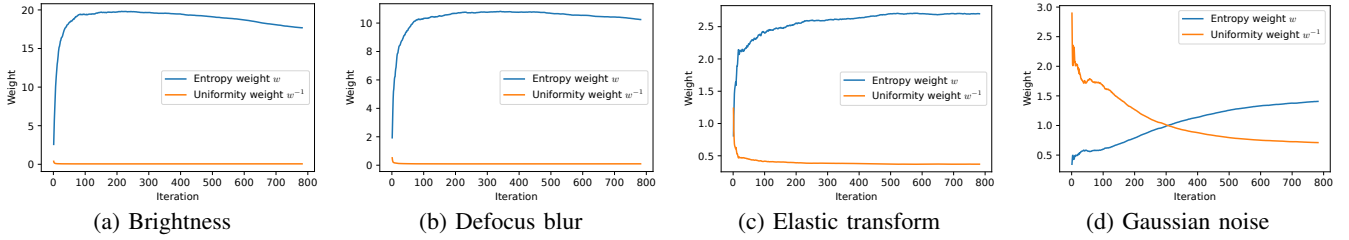


Fig. 3. Evolution of the information-aware loss balancing weights. The weights are adaptively assigned to the entropy and uniformity losses by the difficulty of distribution shifts. A larger weight is assigned to the entropy for easy distribution shifts such as brightness in (a). In contrast, the uniformity loss is first addressed, and then the weight is gradually switched to the entropy for difficult distribution shifts such as Gaussian noise in (d).

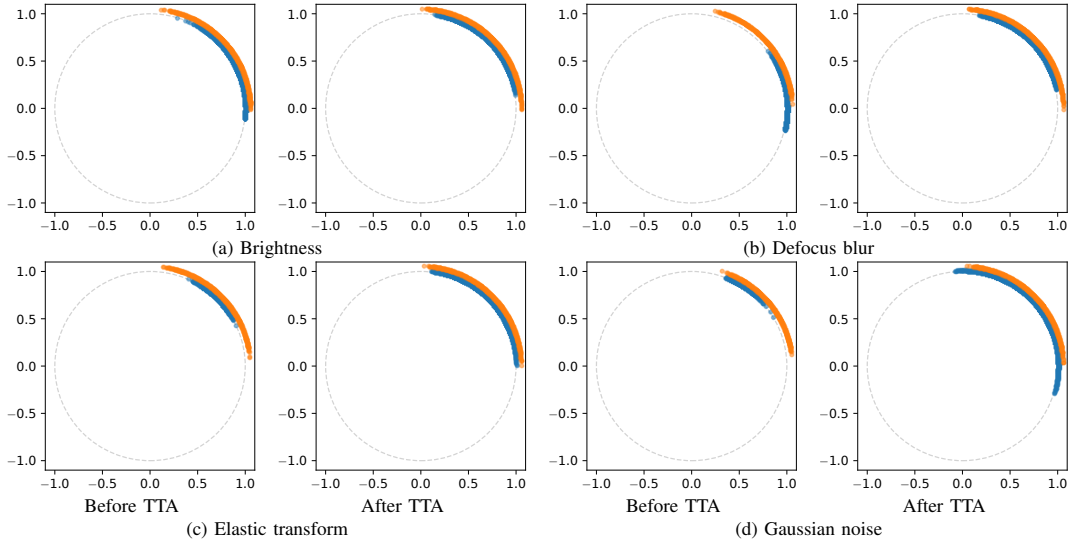


Fig. 4. Spherical PCA [69] visualization of image (blue dots) and text (orange dots) embeddings before and after TTA with UnInfo. The image embeddings are distributed in a broader range of the circle after TTA, which suggests that the uniformity is improved. Moreover, the distribution of the image embeddings is aligned with the text embeddings, i.e., the image embeddings are more classification-friendly.

MTA [19] selects reliable image embeddings and updates the feature centroid. OnZeta [21] and ZERO [68] dynamically correct the prediction probabilities for each test input.

These existing methods can adapt well to domain shifts, such as changes in environments, rendition, OOD [31]–[34], or fine-grained zero-shot classification, such as detailed species classification [35], [36], using fixed image and text encoders. This is because a pre-trained CLIP generalizes to a wide range of domains enough to encode the current domain’s semantics properly. However, these studies do not examine the ability to adapt to another type of distribution shift, sensor degradation. Moreover, we experimentally found that CLIP is vulnerable to this type of distribution shift, and existing methods fail to recover the performance. Updating embeddings has limited representation power for zero-shot classification because updating the final linear layer is equivalent to updating the text embeddings, which are regarded as the weight matrix.

VII. CONCLUSION

We proposed UnInfo, a novel test-time adaptation (TTA) method for zero-shot classification with vision-language models under the sensor degradation. Unlike existing methods, UnInfo updates the image encoder to address the specific challenge of the sensor degradation, where loss input information is retained in the image embeddings unlike other

natural distribution shifts. In the experiments, UnInfo achieved higher classification performance than baselines by refining the uniformity along with the entropy, and the information-aware loss balancing further improved the performance. One limitation of UnInfo is that it requires test data to be mini-batched. Our future work is to extend UnInfo to a fully online setting and broader types of distribution shifts.

REFERENCES

- [1] A. Radford, J. W. Kim, C. Hallacy, A. Ramesh, G. Goh, S. Agarwal, G. Sastry, A. Askell, P. Mishkin, J. Clark *et al.*, “Learning transferable visual models from natural language supervision,” in *International conference on machine learning*. PMLR, 2021, pp. 8748–8763.
- [2] C. Jia, Y. Yang, Y. Xia, Y.-T. Chen, Z. Parekh, H. Pham, Q. Le, Y.-H. Sung, Z. Li, and T. Duerig, “Scaling up visual and vision-language representation learning with noisy text supervision,” in *International conference on machine learning*. PMLR, 2021, pp. 4904–4916.
- [3] Y. Ge, J. Ren, A. Gallagher, Y. Wang, M.-H. Yang, H. Adam, L. Itti, B. Lakshminarayanan, and J. Zhao, “Improving zero-shot generalization and robustness of multi-modal models,” in *Proceedings of the IEEE/CVF conference on computer vision and pattern recognition*, 2023, pp. 11 093–11 101.
- [4] Z. Wang, J. Liang, R. He, N. Xu, Z. Wang, and T. Tan, “Improving zero-shot generalization for clip with synthesized prompts,” in *Proceedings of the IEEE/CVF International Conference on Computer Vision*, 2023, pp. 3032–3042.
- [5] A. Baldrati, M. Bertini, T. Uricchio, and A. Del Bimbo, “Effective conditioned and composed image retrieval combining clip-based features,” in *Proceedings of the IEEE/CVF conference on computer vision and pattern recognition*, 2022, pp. 21 466–21 474.

- [6] H. Fang, P. Xiong, L. Xu, and Y. Chen, "Clip2video: Mastering video-text retrieval via image clip," *arXiv preprint arXiv:2106.11097*, 2021.
- [7] O. Patashnik, Z. Wu, E. Shechtman, D. Cohen-Or, and D. Lischinski, "Styleclip: Text-driven manipulation of stylegan imagery," in *Proceedings of the IEEE/CVF international conference on computer vision*, 2021, pp. 2085–2094.
- [8] A. Ramesh, P. Dhariwal, A. Nichol, C. Chu, and M. Chen, "Hierarchical text-conditional image generation with clip latents," *arXiv preprint arXiv:2204.06125*, vol. 1, no. 2, p. 3, 2022.
- [9] G. Ilharco, M. Wortsman, R. Wightman, C. Gordon, N. Carlini, R. Taori, A. Dave, V. Shankar, H. Namkoong, J. Miller, H. Hajishirzi, A. Farhadi, and L. Schmidt, "OpenCLIP," Jul. 2021.
- [10] M. Cherti, R. Beaumont, R. Wightman, M. Wortsman, G. Ilharco, C. Gordon, C. Schuhmann, L. Schmidt, and J. Jitsev, "Reproducible scaling laws for contrastive language-image learning," in *Proceedings of the IEEE/CVF Conference on Computer Vision and Pattern Recognition*, 2023, pp. 2818–2829.
- [11] C. Schuhmann, R. Beaumont, R. Vencu, C. W. Gordon, R. Wightman, M. Cherti, T. Coombes, A. Katta, C. Mullis, M. Wortsman, P. Schramowski, S. R. Kundurthy, K. Crowson, L. Schmidt, R. Kaczmarczyk, and J. Jitsev, "LAION-5b: An open large-scale dataset for training next generation image-text models," in *Thirty-sixth Conference on Neural Information Processing Systems Datasets and Benchmarks Track*, 2022.
- [12] R. Zhang, R. Fang, W. Zhang, P. Gao, K. Li, J. Dai, Y. Qiao, and H. Li, "Tip-Adapter: Training-free Adaption of CLIP for Few-shot Classification," in *European Conference on Computer Vision (ECCV)*, 2022.
- [13] Y. Huang, F. Shakeri, J. Dolz, M. Boudiaf, H. Bahig, and I. Ben Ayed, "Lp++: A surprisingly strong linear probe for few-shot clip," in *Proceedings of the IEEE/CVF Conference on Computer Vision and Pattern Recognition*, 2024, pp. 23 773–23 782.
- [14] G. Chen, W. Yao, X. Song, X. Li, Y. Rao, and K. Zhang, "PLOT: Prompt learning with optimal transport for vision-language models," in *The Eleventh International Conference on Learning Representations*, 2023.
- [15] S. Manli, N. Weili, H. De-An, Y. Zhiding, G. Tom, A. Anima, and X. Chaowei, "Test-time prompt tuning for zero-shot generalization in vision-language models," in *NeurIPS*, 2022.
- [16] Y. Zhou, J. Ren, F. Li, R. Zabih, and S. N. Lim, "Test-time distribution normalization for contrastively learned visual-language models," *Advances in Neural Information Processing Systems*, vol. 36, 2024.
- [17] A. Karmanov, D. Guan, S. Lu, A. El Saddik, and E. Xing, "Efficient Test-Time Adaptation of Vision-Language Models," in *Proceedings of the IEEE/CVF Conference on Computer Vision and Pattern Recognition*, 2024, pp. 14 162–14 171.
- [18] Y. Zhang, W. Zhu, H. Tang, Z. Ma, K. Zhou, and L. Zhang, "Dual memory networks: A versatile adaptation approach for vision-language models," in *Proceedings of the IEEE/CVF conference on computer vision and pattern recognition*, 2024, pp. 28 718–28 728.
- [19] M. Zanella and I. Ben Ayed, "On the test-time zero-shot generalization of vision-language models: Do we really need prompt learning?" in *Proceedings of the IEEE/CVF Conference on Computer Vision and Pattern Recognition*, 2024, pp. 23 783–23 793.
- [20] Z. Wang, J. Liang, L. Sheng, R. He, Z. Wang, and T. Tan, "A hard-to-beat baseline for training-free CLIP-based adaptation," in *The Twelfth International Conference on Learning Representations*, 2024.
- [21] Q. Qian and J. Hu, "Online zero-shot classification with clip," in *European Conference on Computer Vision*. Springer, 2024, pp. 462–477.
- [22] D. Wang, E. Shelhamer, S. Liu, B. Olshausen, and T. Darrell, "Tent: Fully Test-Time Adaptation by Entropy Minimization," in *International Conference on Learning Representations (ICLR)*, 2021.
- [23] K. Adachi, S. Yamaguchi, and A. Kumagai, "Covariance-Aware Feature Alignment with Pre-Computed Source Statistics for Test-Time Adaptation to Multiple Image Corruptions," in *2023 IEEE International Conference on Image Processing (ICIP)*, 2023, pp. 800–804.
- [24] J. Liang, R. He, and T. Tan, "A comprehensive survey on test-time adaptation under distribution shifts," *International Journal of Computer Vision*, pp. 1–34, 2024.
- [25] K. Zhou, J. Yang, C. C. Loy, and Z. Liu, "Learning to prompt for vision-language models," *International Journal of Computer Vision (IJCV)*, 2022.
- [26] —, "Conditional prompt learning for vision-language models," in *Proceedings of the IEEE/CVF Conference on Computer Vision and Pattern Recognition (CVPR)*, June 2022, pp. 16 816–16 825.
- [27] V. W. Liang, Y. Zhang, Y. Kwon, S. Yeung, and J. Y. Zou, "Mind the gap: Understanding the modality gap in multi-modal contrastive representation learning," *Advances in Neural Information Processing Systems*, vol. 35, pp. 17 612–17 625, 2022.
- [28] M. U. Khattak, H. Rasheed, M. Maaz, S. Khan, and F. S. Khan, "Maple: Multi-modal prompt learning," in *Proceedings of the IEEE/CVF Conference on Computer Vision and Pattern Recognition*, 2023, pp. 19 113–19 122.
- [29] Q. Qian, Y. Xu, and J. Hu, "Intra-modal proxy learning for zero-shot visual categorization with clip," *Advances in Neural Information Processing Systems*, vol. 36, 2024.
- [30] S. Yamaguchi, D. Feng, S. Kanai, K. Adachi, and D. Chijiwa, "Post-pre-training for Modality Alignment in Vision-Language Foundation Models," in *Proceedings of the IEEE/CVF Conference on Computer Vision and Pattern Recognition (CVPR)*, June 2025.
- [31] D. Hendrycks, S. Basart, N. Mu, S. Kadavath, F. Wang, E. Dorundo, R. Desai, T. Zhu, S. Parajuli, M. Guo, D. Song, J. Steinhardt, and J. Gilmer, "The Many Faces of Robustness: A Critical Analysis of Out-of-Distribution Generalization," *arXiv preprint arXiv:2006.16241*, 2020.
- [32] B. Recht, R. Roelofs, L. Schmidt, and V. Shankar, "Do imagenet classifiers generalize to imagenet?" in *International Conference on Machine Learning*. PMLR, 2019, pp. 5389–5400.
- [33] D. Hendrycks, K. Zhao, S. Basart, J. Steinhardt, and D. Song, "Natural Adversarial Examples," in *Proceedings of the IEEE/CVF Conference on Computer Vision and Pattern Recognition (CVPR)*, June 2021, pp. 15 262–15 271.
- [34] H. Wang, S. Ge, Z. Lipton, and E. P. Xing, "Learning Robust Global Representations by Penalizing Local Predictive Power," in *Advances in Neural Information Processing Systems 32*, H. Wallach, H. Larochelle, A. Beygelzimer, F. d'Alché-Buc, E. Fox, and R. Garnett, Eds. Curran Associates, Inc., 2019, pp. 10 506–10 518.
- [35] M.-E. Nilsback and A. Zisserman, "Automated flower classification over a large number of classes," in *Indian Conference on Computer Vision, Graphics and Image Processing*, Dec 2008.
- [36] O. M. Parkhi, A. Vedaldi, A. Zisserman, and C. V. Jawahar, "Cats and dogs," in *IEEE Conference on Computer Vision and Pattern Recognition (CVPR)*, 2012.
- [37] D. Hendrycks and T. Dietterich, "Benchmarking Neural Network Robustness to Common Corruptions and Perturbations," in *Proceedings of the International Conference on Learning Representations (ICLR)*, 2019.
- [38] D. Sójka, S. Cygert, B. Twardowski, and T. Trzcinski, "Ar-tta: A simple method for real-world continual test-time adaptation," in *Proceedings of the IEEE/CVF International Conference on Computer Vision*, 2023, pp. 3491–3495.
- [39] D. Dai and L. V. Gool, "Dark model adaptation: Semantic image segmentation from daytime to nighttime," in *2018 21st International Conference on Intelligent Transportation Systems (ITSC)*, 2018, pp. 3819–3824.
- [40] G. Volk, S. Müller, A. v. Bernuth, D. Hospach, and O. Bringmann, "Towards robust cnn-based object detection through augmentation with synthetic rain variations," in *2019 IEEE Intelligent Transportation Systems Conference (ITSC)*, 2019, pp. 285–292.
- [41] C. Eastwood, I. Mason, C. Williams, and B. Schölkopf, "Source-Free Adaptation to Measurement Shift via Bottom-Up Feature Restoration," in *International Conference on Learning Representations*, 2022.
- [42] K. Adachi, S. Enomoto, T. Sasaki, and S. Yamaguchi, "Test-time similarity modification for person re-identification toward temporal distribution shift," in *2024 International Joint Conference on Neural Networks (IJCNN)*, 2024, pp. 1–8.
- [43] Y. Qin, C. Zhang, T. Chen, B. Lakshminarayanan, A. Beutel, and X. Wang, "Understanding and improving robustness of vision transformers through patch-based negative augmentation," *Advances in Neural Information Processing Systems*, vol. 35, pp. 16 276–16 289, 2022.
- [44] E. Mintun, A. Kirillov, and S. Xie, "On interaction between augmentations and corruptions in natural corruption robustness," in *Advances in Neural Information Processing Systems*, A. Beygelzimer, Y. Dauphin, P. Liang, and J. W. Vaughan, Eds., 2021.
- [45] T. Wang and P. Isola, "Understanding contrastive representation learning through alignment and uniformity on the hypersphere," in *International conference on machine learning*. PMLR, 2020, pp. 9929–9939.
- [46] E. J. Hu, yelong shen, P. Wallis, Z. Allen-Zhu, Y. Li, S. Wang, L. Wang, and W. Chen, "LoRA: Low-rank adaptation of large language models," in *International Conference on Learning Representations*, 2022.
- [47] A. Zhou and S. Levine, "Bayesian Adaptation for Covariate Shift," *Advances in Neural Information Processing Systems*, vol. 34, 2021.

- [48] S. Niu, J. Wu, Y. Zhang, Y. Chen, S. Zheng, P. Zhao, and M. Tan, "Efficient test-time model adaptation without forgetting," in *International conference on machine learning*. PMLR, 2022, pp. 16 888–16 905.
- [49] M. Zhang, S. Levine, and C. Finn, "Memo: Test time robustness via adaptation and augmentation," *Advances in neural information processing systems*, vol. 35, pp. 38 629–38 642, 2022.
- [50] S. Enomoto, N. Hasegawa, K. Adachi, T. Sasaki, S. Yamaguchi, S. Suzuki, and T. Eda, "Test-time adaptation meets image enhancement: Improving accuracy via uncertainty-aware logit switching," in *2024 International Joint Conference on Neural Networks (IJCNN)*, 2024, pp. 1–8.
- [51] A. Hurst, A. Lerer, A. P. Goucher, A. Perelman, A. Ramesh, A. Clark, A. Ostrow, A. Welihinda, A. Hayes, A. Radford *et al.*, "Gpt-4o system card," *arXiv preprint arXiv:2410.21276*, 2024.
- [52] J. Deng, W. Dong, R. Socher, L.-J. Li, K. Li, and L. Fei-Fei, "Imagenet: A large-scale hierarchical image database," in *The IEEE Conference on Computer Vision and Pattern Recognition (CVPR)*, 2009, pp. 248–255.
- [53] A. v. d. Oord, Y. Li, and O. Vinyals, "Representation learning with contrastive predictive coding," *arXiv preprint arXiv:1807.03748*, 2018.
- [54] J. Bridle, A. Heading, and D. MacKay, "Unsupervised Classifiers, Mutual Information and 'Phantom Targets,'" in *Advances in Neural Information Processing Systems*, J. Moody, S. Hanson, and R. P. Lippmann, Eds., vol. 4. Morgan-Kaufmann, 1992.
- [55] A. Krause, P. Perona, and R. Gomes, "Discriminative Clustering by Regularized Information Maximization," in *Advances in Neural Information Processing Systems*, J. Lafferty, C. Williams, J. Shawe-Taylor, R. Zemel, and A. Culotta, Eds., vol. 23. Curran Associates, Inc., 2010. [Online]. Available: <https://proceedings.neurips.cc/paper/2010/file/42998cf32d552343bc8e460416382dca-Paper.pdf>
- [56] Y. Shi and F. Sha, "Information-theoretical learning of discriminative clusters for unsupervised domain adaptation," in *International Conference on Machine Learning (ICML)*, 2012.
- [57] W. Hu, T. Miyato, S. Tokui, E. Matsumoto, and M. Sugiyama, "Learning discrete representations via information maximizing self-augmented training," in *International Conference on Machine Learning (ICML)*, ser. Proceedings of Machine Learning Research, D. Precup and Y. W. Teh, Eds., vol. 70. PMLR, 06–11 Aug 2017, pp. 1558–1567.
- [58] Z. Lai, N. Vedapant, N. Zhou, J. Wu, C. P. Huynh, X. Li, K. K. Fu, and C.-N. Chuah, "Padclip: Pseudo-labeling with adaptive debiasing in clip for unsupervised domain adaptation," in *Proceedings of the IEEE/CVF International Conference on Computer Vision (ICCV)*, October 2023, pp. 16 155–16 165.
- [59] N. Vedapant, K. K. Fu, Y. Wu, X. Zhang, and P. Natarajan, "HVCLIP: High-dimensional vector in CLIP for unsupervised domain adaptation," in *European Conference on Computer Vision (ECCV)*, 2024, pp. 36–54.
- [60] M. Zanella and I. Ben Ayed, "Low-rank few-shot adaptation of vision-language models," in *Proceedings of the IEEE/CVF Conference on Computer Vision and Pattern Recognition (CVPR) Workshops*, June 2024, pp. 1593–1603.
- [61] Q. Wang, O. Fink, L. Van Gool, and D. Dai, "Continual test-time domain adaptation," in *Proceedings of the IEEE/CVF Conference on Computer Vision and Pattern Recognition (CVPR)*, June 2022, pp. 7201–7211.
- [62] Y. Gao, X. Shi, Y. Zhu, H. Wang, Z. Tang, X. Zhou, M. Li, and D. N. Metaxas, "Visual prompt tuning for test-time domain adaptation," *arXiv preprint arXiv:2210.04831*, 2022.
- [63] M. Döbler, R. A. Marsden, and B. Yang, "Robust mean teacher for continual and gradual test-time adaptation," in *Proceedings of the IEEE/CVF Conference on Computer Vision and Pattern Recognition (CVPR)*, June 2023, pp. 7704–7714.
- [64] Y. Wang, J. Hong, A. Cheraghian, S. Rahman, D. Ahmedt-Aristizabal, L. Petersson, and M. Harandi, "Continual test-time domain adaptation via dynamic sample selection," in *Proceedings of the IEEE/CVF Winter Conference on Applications of Computer Vision (WACV)*, January 2024, pp. 1701–1710.
- [65] S. Y. Gadre, G. Ilharco, A. Fang, J. Hayase, G. Smyrnis, T. Nguyen, R. Marten, M. Wortsman, D. Ghosh, J. Zhang *et al.*, "Datacomp: In search of the next generation of multimodal datasets," *Advances in Neural Information Processing Systems*, vol. 36, 2024.
- [66] I. Loshchilov and F. Hutter, "Decoupled weight decay regularization," in *International Conference on Learning Representations*, 2019.
- [67] K. He, X. Zhang, S. Ren, and J. Sun, "Delving deep into rectifiers: Surpassing human-level performance on imagenet classification," in *Proceedings of the IEEE International Conference on Computer Vision (ICCV)*, December 2015.
- [68] M. Farina, G. Franchi, G. Iacca, M. Mancini, and E. Ricci, "Frustratingly easy test-time adaptation of vision-language models," in *The Thirty-eighth Annual Conference on Neural Information Processing Systems*, 2024.
- [69] K. Liu, Q. Li, H. Wang, and G. Tang, "Spherical principal component analysis," in *Proceedings of the 2019 SIAM International Conference on Data Mining*. SIAM, 2019, pp. 387–395.
- [70] X. Chen, H. Fang, T.-Y. Lin, R. Vedantam, S. Gupta, P. Dollár, and C. L. Zitnick, "Microsoft coco captions: Data collection and evaluation server," *arXiv preprint arXiv:1504.00325*, 2015.
- [71] H. S. Yoon, E. Yoon, J. T. J. Tee, M. Hasegawa-Johnson, Y. Li, and C. D. Yoo, "C-TPT: Calibrated Test-Time Prompt Tuning for Vision-Language Models via Text Feature Dispersion," in *International Conference on Learning Representations (ICLR)*, 2024.

APPENDIX

TEXT PROMPT ENSEMBLE

Here, we describe the details of the prompt ensemble in the preliminary experiment (Section III). We used template texts listed in Table VIII for the ensemble of multiple templates (denoted by "Ensemble" in Table I). We generated the prompts using the templates for each class and encoded them with the text encoder. Then, we calculated the mean of the text embeddings. We normalized the embedding and used it for the class prototype.

For the ensemble of corruption synonyms (denoted by "Corruption prompt" in Table I), we ensembled the corruption synonyms listed in Table IX, which are generated by GPT-4o [51] with the instruction "You are an expert of image processing. List the synonyms of the word "[corruption name]," which represents image quality."

⁴https://github.com/openai/CLIP/blob/main/notebooks/Prompt_Engineering_for_ImageNet.ipynb

TABLE VIII
TEXT PROMPT TEMPLATES USED FOR ENSEMBLE IN THE PRELIMINARY EXPERIMENT (SECTION III). THESE TEMPLATES ARE PROPOSED BY RADFORD ET AL. [1]⁴.

a bad photo of a {}.	a photo of many {}.	a sculpture of a {}.	a photo of the hard to see {}.
a low resolution photo of the {}.	a rendering of a {}.	graffiti of a {}.	a bad photo of the {}.
a cropped photo of the {}.	a tattoo of a {}.	the embroidered {}.	a photo of a hard to see {}.
a bright photo of a {}.	a photo of a clean {}.	a photo of a dirty {}.	a dark photo of the {}.
a drawing of a {}.	a photo of my {}.	the plastic {}.	a photo of the cool {}.
a close-up photo of a {}.	a black and white photo of the {}.	a painting of the {}.	a painting of a {}.
a pixelated photo of the {}.	a sculpture of the {}.	a bright photo of the {}.	a cropped photo of a {}.
a plastic {}.	a photo of the dirty {}.	a jpeg corrupted photo of a {}.	a blurry photo of the {}.
a photo of the {}.	a good photo of the {}.	a rendering of the {}.	a {} in a video game.
a photo of one {}.	a doodle of a {}.	a close-up photo of the {}.	a photo of a {}.
the origami {}.	the {} in a video game.	a sketch of a {}.	a doodle of the {}.
a origami {}.	a low resolution photo of a {}.	the toy {}.	a rendition of the {}.
a photo of the clean {}.	a photo of a large {}.	a rendition of a {}.	a photo of a nice {}.
a photo of a weird {}.	a blurry photo of a {}.	a cartoon {}.	art of a {}.
a sketch of the {}.	a embroidered {}.	a pixelated photo of a {}.	itap of the {}.
a jpeg corrupted photo of the {}.	a good photo of a {}.	a plushie {}.	a photo of the nice {}.
a photo of the small {}.	a photo of the weird {}.	the cartoon {}.	art of the {}.
a drawing of the {}.	a photo of the large {}.	a black and white photo of a {}.	the plushie {}.
a dark photo of a {}.	itap of a {}.	graffiti of the {}.	a toy {}.
itap of my {}.	a photo of a cool {}.	a photo of a small {}.	a tattoo of the {}.

TABLE IX
SYNONYMS OF THE CORRUPTION NAMES OF IMAGENET-C USED IN THE PRELIMINARY EXPERIMENT IN SECTION III.

Defocus blur	Glass blur	Motion blur	Zoom blur	Contrast
defocus blur	glass blur	motion blur	zoom blur	contrast
out-of-focus blur	frosted blur	directional blur	radial blur	tonal contrast
soft focus	glazing blur	linear blur	zooming effect	brightness difference
bokeh	diffuse blur	dynamic blur	dynamic zoom blur	clarity
lens blur	smudged blur	streaking	burst blur	definition
gaussian blur	hazy blur	trail blur	focus expansion blur	distinction
depth blur	translucent blur	speed blur	depth blur	sharpness
background blur	refractive blur	panning blur	lens zoom blur	intensity difference
field blur	distortion blur	motion streak	outward motion blur	dynamic range
focus softness	veiled blur	kinetic blur	radian streak blur	separation
Elastic transform	Jpeg compression	Pixelate	Gaussian noise	Impulse noise
elastic transform	jpeg compression	pixelate	Gaussian noise	impulse noise
warping	image compression	blockify	normal noise	salt-and-pepper noise
distortion	lossy compression	rasterize	additive noise	spiky noise
deformation	JPEG encoding	mosaic	white Gaussian noise	outlier noise
stretching	file compression	chunkify	statistical noise	random noise
bending	quantization artifacting	grid effect	random noise	shot noise
geometric transform	data compression	quantization	luminance noise	transitional noise
morphing	image encoding	low-resolution effect	stochastic interference	burst noise
image warping	compression artifacts	bitmapping	signal perturbation	pulsed noise
spatial transform	JPEG artifacts	aliased effect	normal distribution noise	point noise
Shot noise	Brightness	Fog	Frost	Snow
shot noise	brightness	fog	frost	snow
photon noise	luminance	haze	frosting	noise
Poisson noise	illumination	mist	glare	grain
quantum noise	lightness	obscuration	haze	salt-and-pepper noise
statistical noise	intensity	cloudiness	mist	static
random noise	radiance	smog	veiling	visual noise
electronic noise	glow	blur	soft-focus	pixel noise
counting noise	shininess	glare	diffusion	random noise
current noise	exposure	veiling	cloudiness	white noise
flicker noise	highlighting	dimming	blur	dither